REDUCTION OF DIFFUSION-WEIGHTED READOUT-SEGMENTED EPI SCAN TIME USING A BLIPPED-CAIPI MODIFICATION

Robert Frost[1], David A. Porter[2], Gwenaelle Douaud[1], Peter Jezzard[1], and Karla L. Miller[1]
[1]*FMRIB Centre, Nuffield Department of Clinical Neurosciences, University of Oxford, Oxford, United Kingdom,* [2]*Healthcare Sector, Siemens AG, Erlangen, Germany*

Introduction Readout-segmented EPI (rs-EPI) is an alternative to single-shot EPI (ss-EPI) that reduces distortion and T2* blurring, enabling higher spatial resolution. For diffusion imaging, rs-EPI includes navigator correction and reacquisition of motion-corrupted shots (1-4). k-space is segmented in the readout (k_x) direction, enabling short echo-spacing (low distortion) at the cost of longer scan times, placing an effective limit on slices and/or diffusion directions. Faster scan time for rs-EPI can only be achieved by reducing the effective number of k-space segments. Partial Fourier (PF) can reduce the number of segments per slice (5), but reduces SNR and has limited scan time reduction (≤40%). Here, we use multiband excitations, which effectively shares readout segments across slices. Simultaneously-excited slices are separated based on coil sensitivity profiles and incur an SNR reduction that depends only on g-factor (6), which can be improved through careful control of the aliasing pattern (7). Here, we demonstrate multiband rs-EPI for both trace-weighted and multi-direction diffusion acquisition and compare tractography results with ss-EPI.

Methods Data were acquired with both multislice and in-slice accelerations. A multiband RF pulse (phase-modulated sum-of-sincs) excited R=2 slices with slice separation S. One slice was shifted by FOV/2 using blipped-CAIPI (8) to minimize g-factor SNR loss. The GRAPPA kernel used to separate slices is calculated from reference data with single-slice excitation (b=0). For long DTI scans, reference acquisitions are interleaved with diffusion directions to minimize artifacts due to subject motion. Off-line reconstruction included phase correction of off-isocentre slices, regridding and ghost correction. The slice-GRAPPA reconstruction (8) uses separate kernels for each slice (calculated from the central segments of the multiband b=0 and reference data). The standard rs-EPI reconstruction pipeline was then applied to produce the final image: in-plane GRAPPA (9) (acceleration R_{PE}), nonlinear navigator correction, segment concatenation and sum-of-squares coil combination.

Experiments Data were acquired using a 32-ch receive coil on a Siemens Verio 3T scanner. Diffusion weighting was achieved with a single-refocused spin-echo for rs-EPI and twice-refocused for ss-EPI (due to the greater sensitivity of ss-EPI to eddy currents). Motion corruption was monitored in real-time, and 20% of the rs-EPI scan time was dedicated to reacquiring corrupted segments. Two rs-EPI DTI protocols were acquired with FOV=220×220mm^2, R_{PE}=2 and with 60 b=1000s/mm^2 directions and 12 volumes without diffusion-weighting as follows: *2mm iso rs-EPI DTI protocol*: # slices=58; matrix=110×110; TR/TE=4.1s/73ms; 5 readout segments; scan time=33min for full k-space acquisition; total reference time=2min. *1.5mm iso rs-EPI DTI protocol*: # slices=62; matrix=144×144; TR/TE=4.8s/79ms; 7 readout segments; scan time=51min for full k-space acquisition; total reference time=2:42min. *rs-EPI DWI protocol*: res=0.9×0.9×4mm; # slices=30; matrix=256×256; TR/TE=3s/76ms; 11 readout segments; 1 b=0 and 3 orthogonal b=1000s/mm^2 directions; scan time=2:50min for full k-space acquisition; total reference time=30s. Two ss-EPI DTI protocols were acquired with phase-encode PF=6/8, FOV=190×190mm^2, R_{PE}=2, 60 b=1000s/mm^2 directions and 12 volumes without diffusion-weighting and 3 averages as follows: *2mm iso ss-EPI DTI protocol*: # slices=58; matrix=96×96; TR/TE=8.4s/87ms; scan time=34min. *1.5mm iso ss-EPI DTI protocol*: # slices=62; matrix=128×128; TR/TE=13.9s/88ms; scan time=54min. *Data processing*: Brain extraction, eddy current correction, diffusion tensor fitting and tractography was performed using FSL (www.fmrib.ox.ac.uk/fsl/). Tractography seed masks were drawn in the subject's structural space for several tracts, including association, commissural and projection fibers: superior longitudinal fasciculus (SLF), cingulum bundle, optic tract, fornix, corpus callosum (CC) and corticospinal tract (CST).

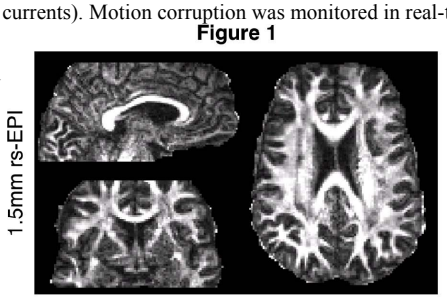

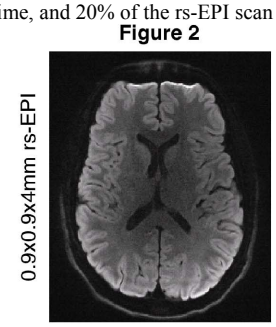

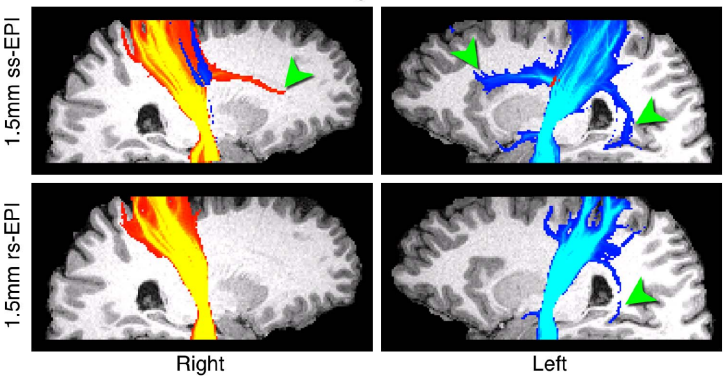

Results Figures 1 and 2 demonstrate image quality for multiband rs-EPI: fractional anisotropy at 1.5mm isotropic resolution and trace-weighted imaging for 0.9×0.9×4mm. Both datasets demonstrate low levels of distortion at relatively high resolution, consistent with previous rs-EPI results, but importantly achieve whole-brain coverage in reasonable scan times. Tractography generally improved at 1.5mm compared to 2mm in both the rs- and ss-EPI, producing more true positives and fewer false positives (data not shown). For example, unlike for 2mm rs- and ss-EPI, tractography seeded in the anterior pillars of the fornix correctly tracked into the hippocampus and did not mistrack into the anterior commisure in the 1.5mm data. Overall, tractography in the 1.5mm rs- and ss-EPI data sets was comparable in terms of the ratio of true- to false- positives (correct vs. incorrect tracts). However, the streamlines generally died out earlier in the rs-EPI data, such that the total number of streamlines reaching cortex (whether correct or incorrect) was greater in ss-EPI. One example where the rs-EPI did yield improved tractography is the CST. Maximum intensity projections (within-hemisphere) of the CST are shown in Fig. 3 overlaid onto representative slices of the structural image. Streamlines from the right and left hemisphere seeds are shown in red-yellow and blue, respectively, at the same threshold (>100 streamlines). The ss-EPI mistracks into anterior regions via the SLF (arrows), while the rs-EPI delineates the CST projections into M1 and S1 cortex much more cleanly.

Discussion This study demonstrates that a blipped-CAIPI multiband modification is compatible with the rs-EPI sequence and in particular, with multishot navigator correction. In the rs-EPI approach, minor motion corruption (outside of systole) is removed by the nonlinear navigator correction, while segments with more significant corruption (during systole) are simply re-acquired. The navigator-based reacquisition was able to identify the shots with the most motion corruption based on the sum of the navigator signals from the simultaneously acquired slices. Lower slices in the brain suffer the worst motion artifact (3), so as the number of simultaneously acquired slices is increased it may be necessary to consider individual receive channels in a more detailed way to sensitively detect dropout in individual slices.

The blipped-CAIPI multiband modification proposed here is expected to address one of the major current shortcomings of rs-EPI. Acquisition of whole-brain high-resolution trace-weighted data in clinically relevant scan times is now possible, as are measurements with a large number of diffusion directions. The tractography resolution demonstrated in this study clearly demonstrates the feasibility of tractography with rs-EPI, although streamlines with ss-EPI had a greater tendency to reach cortex. This likely reflects higher SNR in ss-EPI, potentially due to imperfections in rs-EPI or ss-EPI blurring from the simple PF reconstruction. Nevertheless, higher resolution in all cases improved tractography, and it is thus significant that rs-EPI does not suffer from the distortion-resolution tradeoff that limits ss-EPI. High resolution does still pose an SNR challenge, which may motivate higher acceleration factors to increase SNR efficiency and/or higher field strength. In this study the slice acceleration was limited by the peak RF voltage/SAR of the summed RF pulses which could be mitigated with a more sophisticated RF pulse design.

Acknowledgements We are grateful to Thorsten Feiweier for providing the monopolar diffusion preparation module used in rs-EPI and for funding from the Medical Research Council. References (1) Robson MRM 1997;38. (2) Porter MRM 2009;62. (3) Miller MRM 2003;50. (4) Nguyen ISMRM 1998. (5) Frost MRM 2011. (6) Larkman JMRI 2001;13. (7) Breuer MRM 2005;53. (8) Setsompop MRM 2011. (9) Griswold MRM 2002;47.